Research Article

Microstructural properties and antibacterial activity of Ce doped NiO through chemical method

M. Abdur Rahman[1] · **R. Radhakrishnan**[2]

Abstract
The nickel oxide and different concentration of Cerium ions (0.01 M, 0.02 M and 0.03 M) doped NiO nanoparticles (NPs) were synthesized by chemical method. The XRD spectra exhibited the cubic structure of NiO. The average crystalline sizes were observed as 43 nm, 36 nm, 29 nm and 23 nm in NiO and Ce doped NiO NPs, respectively. The Ni (2p), O (1s) and Ce (3d) oxidation states were confirmed by XPS spectra. The FESEM image and TEM image showed the flowers with spherical nanostructure in undoped and doped NiO NPs. The Chemical compositions were identified by EDAX spectra. Metal-oxide (Ni–O) functional groups were found at 439, 435, 445 and 446 cm^{-1} in undoped and doped samples respectively. The optical studies were carried out using UV–Vis spectra and PL studies. Magnetization values were enhanced in Ce doped NiO NPs as compared to NiO NPs. Antibacterial activities were done by various human pathogens with using NiO and Ce doped NiO NPs.

Keywords NiO NPs · Ce doped NiO NPs · XRD · PL · Oxygen vacancies · VSM · Antibacterial activity

1 Introduction

Rare earth (RE) 3d ion doped with NiO has been intensively studied in the past decade, to obtain better optical and magnetic properties [1]. RE atoms are possessing the special 4f shells. RE atoms are the excellent candidates for the luminescence centers of doped materials due to the transition of intra –4f or 4f–5d narrow emission line. The transition plays the important roles in the absorption of RE atoms in the UV range. An energy transfer process from the excited semiconductor host to doping lanthanide atoms, promoted the doped NPs to circumvent absorption of optical centers with extraordinary improvement of luminescent properties [2, 3]. Cerium as one element of Lanthanide doped semiconductors has been used in the focus of numerous unique potential applications like optical properties and biomedical applications [4–8]. The NiO NPs are p-type semiconductors and have stable wide band gap (3.4–4.0 eV) [9]. The NiO NPs are one of the promising metal oxides for various potential applications like alkaline batteries, gas sensors, electrochemical capacitors, smart windows, biomedicine, drug delivery, and magnetic bar codes [10–15].

The mechanism of antibacterial actions of the material states were productions of reactive oxygen species (ROS) [16] on the surface of these NPs in the light causes oxidative stress in bacterial cells eventually, leading to death of the cells. Reactive oxygen species contain the most reactive hydroxyl radical (OH), the less toxic superoxide anion radical ($^{\cdot}O_2^-$) and hydrogen peroxide with a weaker oxidizer (H_2O_2). This can damage Deoxyribo nucleic acid (DNA), cell membranes, etc., which lead to cell death [17]. The attachment of the NPs to the bacteria has also been demonstrated. This is attributed to the electrostatic attraction between the negatively charged bacteria and the positively charged NPs. Such a contact may not only

✉ M. Abdur Rahman, abdur84@gmail.com | [1]PG and Research Department of Physics, Sudharsan College of Arts and Science, Pudukkottai, Tamilnadu 622 104, India. [2]PG and Research Department of Physics, Jamal Mohamed College (Autonomous), Tiruchirapalli, Tamilnadu 620 020, India.

SN Applied Sciences (2019) 1:221 | https://doi.org/10.1007/s42452-019-0232-y

Received: 18 August 2018 / Accepted: 6 February 2019 / Published online: 11 February 2019

inhibit bacterial growth, but also the generated reactive oxygen species may kill the cell [18]. It suggests that both NiO NPs and Ni^{2+} are toxic, but have different modes of actions which take place in the antibacterial cell death.

In the present investigations, NiO (A1), [cerium] Ce^{3+} ions (0.01 M (A2), 0.02 M (A3) and 0.03 M (A4)) doped NiO samples are synthesized by chemical method. The Synthesized samples are studied in structural, optical, magnetic and antibacterial properties of A1, A2, A3 and A4 samples and examined.

2 Materials and method

Nickel (II) nitrate hexahydrate (AR), cerium (III) nitrate hexahydrate (AR) and NaOH (AR) were used as precursor materials for the synthesis of $Ni_{1-x}Ce_xO$ (where x = 0.0, 0.01, 0.02 and 0.03) series.

The experimental procedure for the preparation of NiO NPs (A1) sample has been reported in our previous paper [1]. In the case of Ce doped NiO samples, the synthesis of $Ni_{1-x}Ce_xO$ (x = 0.01 M (A2), 0.02 M (A3) and 0.03 M (A4)) of cerium nitrate salt solution was mixed with Nickel nitrate solution. 0.8 M of NaOH solution was added in drops to the homogenous mixed metal solution to form a black precipitate. The black precipitate was washed a number of times with deionized water and ethanol. Further the black precipitate was dried at 120 °C for 1 h. The obtained Ce doped NiO samples were annealed at 700 °C for 5 h and used for further studies.

The antibacterial activities of the $Ni_{1-x}Ce_xO$ NPs for x = 0.0 (A1), 0.01 M (A2), 0.02 M (A3) and 0.03 M (A4) were investigated by the well diffusion method. They have been reported in our previous paper [1].

2.1 Characterization techniques

The NiO NPs were characterized by X-ray (XRD) diffractometer (model: X'PERT PRO PANalytical). The diffraction patterns were recorded in the range of 20°–80°. The monochromatic wavelength of 1.54Å was used. The XPS measurements were performed with an XPS (Carl Zeiss) equipment. The spectra were at a pressure using an ultra high vacuum with Al Kα excitation at 250 W. The samples were analyzed by Field Emission Scanning Electron (FESEM) Microscopy (Carl Zeiss Ultra 55 FESEM) with EDAX (model: Inca). FT-IR spectra were recorded with using Perkin-Elmer spectrometer. The UV–Vis-NIR spectrum was recorded in the wavelength range 190–1110 nm using Lambda 35. The magnetic properties were analyzed by vibrating sample magnetometer (Lakeshore mini VSM 3639).

3 Results and discussion

The synthesized NiO and Ce doped NiO NPs is formed as a cubic structure (Fig. 1), which is well matched with JCPDS card no.: 01-175-0269 (space group Fm3m) without any CeO_2 and Ce_2O_3. Characteristic peaks of impurities shifted in slight higher angle (2θ) for A2, A3 and A4 samples as compared to that of A1 samples (Fig. 2).The estimated lattice constant (a), unit cell volume (V) and crystallite size (D) values are (4.182 Å, 4.179Å, 4.166 Å and 4.162 Å), (73.139 $Å^3$ 72.982 $Å^3$, 72.303 $Å^3$ and 72.095 $Å^3$) and (43 nm, 36 nm, 29 nm and 23 nm) for A1, A2, A3 and A4 samples respectively, those changes may be due to the substitution Ce^{3+} ions into NiO matrix.

Figure 3a–c shows that Ni (2p), O (1s) and Ce (3d) oxidation state are studied for $Ni_{0.98}Ce_{0.02}O$ NPs using XPS spectra. The Ni ($2p_{3/2}$) and Ni ($2p_{1/2}$) peaks are (879.63 eV, 871.91 eV, 866.02 eV, 860.90 eV, 855.36 eV and 853.60 eV), respectively due to Ni^{2+} of NiO and satellite, shakeup structure for A3 NPs [19, 20]. Figure 3b shows Ce 3d state splits into three signals are observed at (879.34 eV, 898.42 eV and 906.40 eV) respectively. The Ce 3d state peaks are found at 898.42 eV for Ce^{4+} $3d_{5/2}$ oxidation states and in

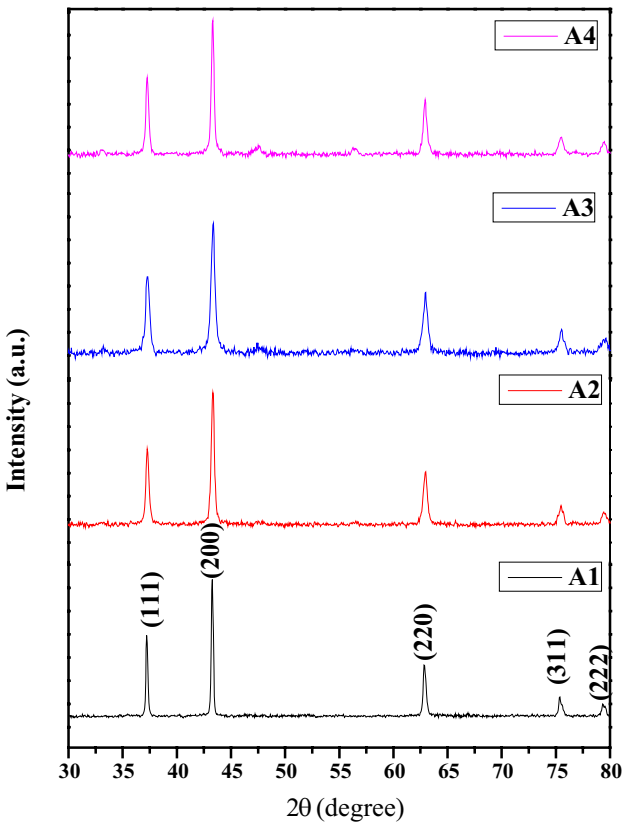

Fig. 1 X-ray diffraction pattern of $Ni_{1-x}Ce_xO$ nanoparticles for x = 0.0, 0.01, 0.02 and 0.03

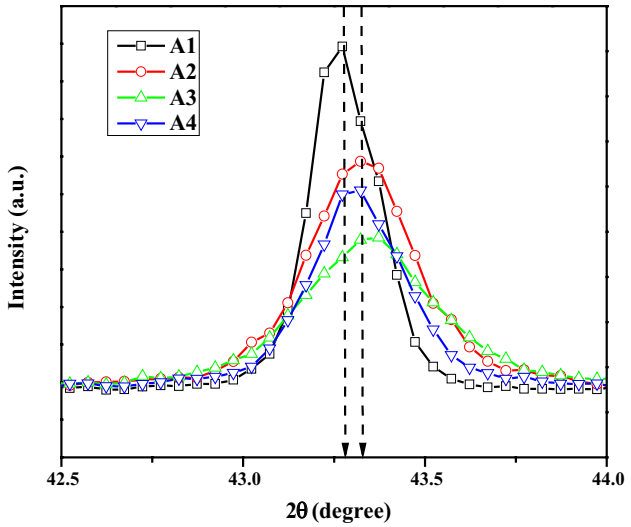

Fig. 2 X-ray powder diffraction patterns of doping-induced peak shift for NiO and Ce doped NiO nanoparticles

addition two satellite Ce^{3+} ($3d_{3/2}$) and Ce^{3+}($3d_{5/2}$) states located at 906.40 eV and 879.34 eV for Ce doped NiO nanoparticles. The O (1s) signals are located at 529.26 eV, 530.91 eV and 532.25 eV in Ce doped NiO NPs, this is due to the O^{2-} in NiO NPs. The atomic percentages of the samples are shown in Table 1.

The FESEM image showed the topography of A1, A2, A3 and A4 samples are shown in Fig. 4a–d. The nanoflower structure with uniform grain boundaries are found in the pure NiO nanoparticles. The Ce doped NiO NPs are exhibited in the spherical structure. Increasing with Ce concentration also decreased with spherical structure in NiO nanoparticles. These topographical changes are due to Ce^{3+} ion substitution into NiO matrix. The average crystal sizes are observed in nanoscale range 25–65 nm for NiO and Ce doped NiO nanoparticles.

The TEM images showed the morphology of NiO and $Ni_{0.97}Ce_{0.03}O$ NPs samples are shown in Fig. 5a, b. The Nanoflower and spherical structure for NiO and $Ni_{0.97}Ce_{0.03}O$ NPs. Figure 6a–d showed the elemental composition of A1, A2, A3 and A4 samples were identified by the energy dispersive analysis of x-ray (EDAX) spectral analysis. In the case of Ce doped NiO samples, the Ce^{3+} ion atomic percentage are observed at 0.60%, 1.29% and 1.67%. In NiO samples, the chemical compositions of Ni and O are found to be 55.49% and 44.51% (Table 2) respectively. However, in Ce doped NiO samples, the Ni percentage decreased whereas the oxygen percentage increased.

A FT-IR spectrum is an easier tool for understanding the functional groups. Figure 7 shows the IR spectra of NiO and various concentrations of Ce doped NiO nanoparticles. The broad O–H stretching peaks are observed at 3335, 3450, 3446 and 3444 cm^{-1} for NiO and Ce doped NiO

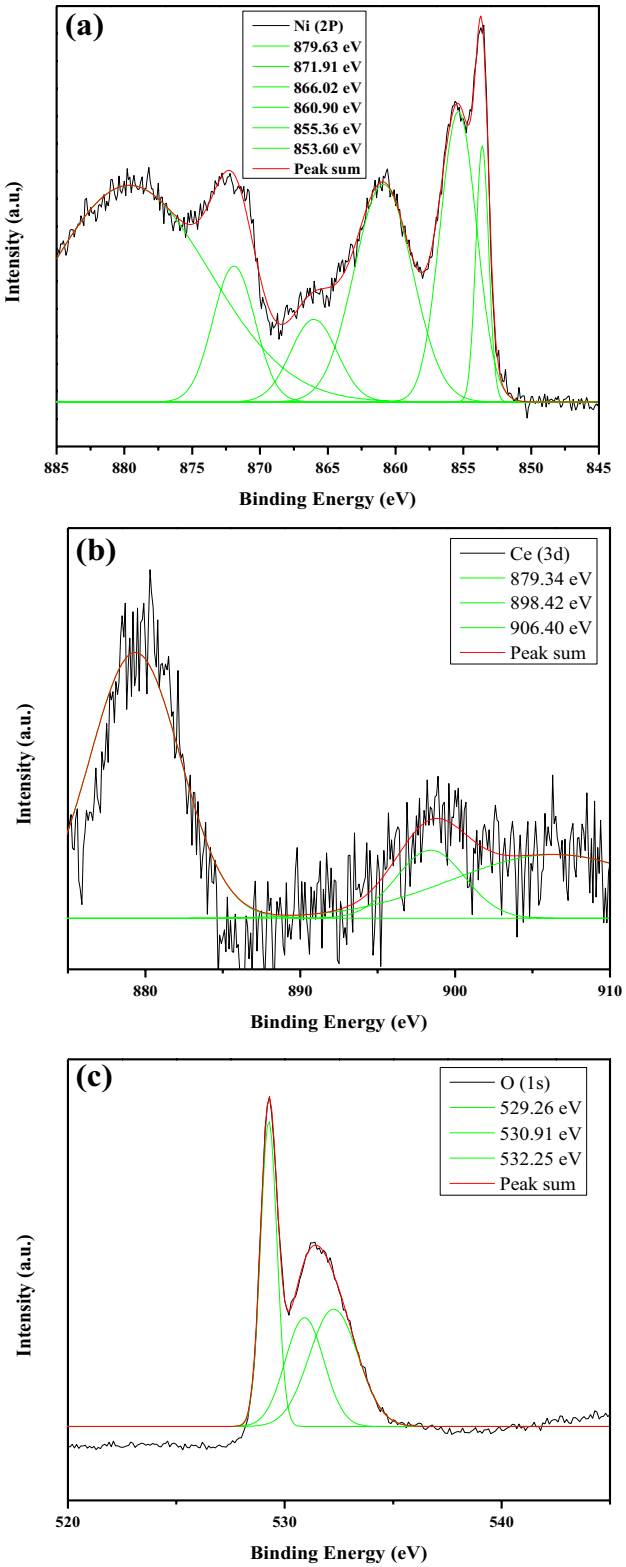

Fig. 3 XPS spectra of **a** Ni (2p), **b** O (1s) and **c** Ce (3d) oxidation state of Ce doped NiO nanoparticles

Table 1 Atomic percentage of Ce doped NiO NPs

Ni 2p	O 1s	Doping %
Atom. Con %	Atom. Con %	Atom. Con %
36.14	62.62	1.24 (Ce 3d)

nanoparticles respectively [21] The week C–H symmetric and asymmetric stretching centered at (2838, 2886 and 2885 cm^{-1}) and (2971, 2944 and 2924 cm^{-1}) were observed in both NiO nanoparticles. The O–H bending vibration observed at 1647, 1641, 1638 and 1635 cm^{-1} for NiO and Ce doped NiO NPs respectively, which is attributed to the adsorbed water on the surface of NPs [22]. The absorption peaks observed at 417, 415, 417 and 412 cm^{-1} corresponds to Ni–O stretching vibration of NiO NPs. The absorption peaks observed at 1647, 1636, 1638 and 1636 cm^{-1} are attributed to the bending mode H–O-H of water molecules for all NiO nanoparticles. The Ni–O stretching bands are observed at 439, 435, 445, and 446 cm^{-1} in NiO and Ce doped NiO nanoparticles [23].

The ultra violet visible (UV–Vis) absorption spectra and the absorption edge peaks are located at 346, 322 nm, 318 nm and 328 nm (Fig. 8) for A1, A2, A3 and A4 samples. The Ce^{3+} ions substituted into NiO matrix, due to the varying of the optical properties. This result, absorption peaks edge values decreased with increasing Ce^{3+} ions concentration. The optical band gap (E_g) can be calculated by Tauc relation [24]. The optical band gap was observed at 2.65 ± 0.1 eV, 2.8 ± 0.1 eV, 2.85 ± 0.1 eV and 2.9 ± 0.1 eV (Fig. 9) for A1, A2, A3 and A4 samples. The Blue shift of absorption and the increasing band gap of Ce doped NiO nanoparticles are evidence of the quantum confinement effect. The trends of the band gap energy value increased due to the decrease in the crystalline size for Ce doped NiO NPs. The corresponding effects are also reflected in the x-ray powder diffraction (XRD) result due to Ce^{3+} ion substitution effects.

Figure 10 shows that a PL spectrum of A1, A2, A3 and A4 samples with excited wavelength is 320 nm. The pure NiO nanoparticles PL emission values are observed at 364 nm, 439, 481 nm and 527 nm respectively. The strong near band edge emission is centered at 364 nm, which is due to the recombination of excitons. The blue emission located at 439 and 481 nm is attributed to the surface oxygen vacancies of NiO NPs. The green emission bands

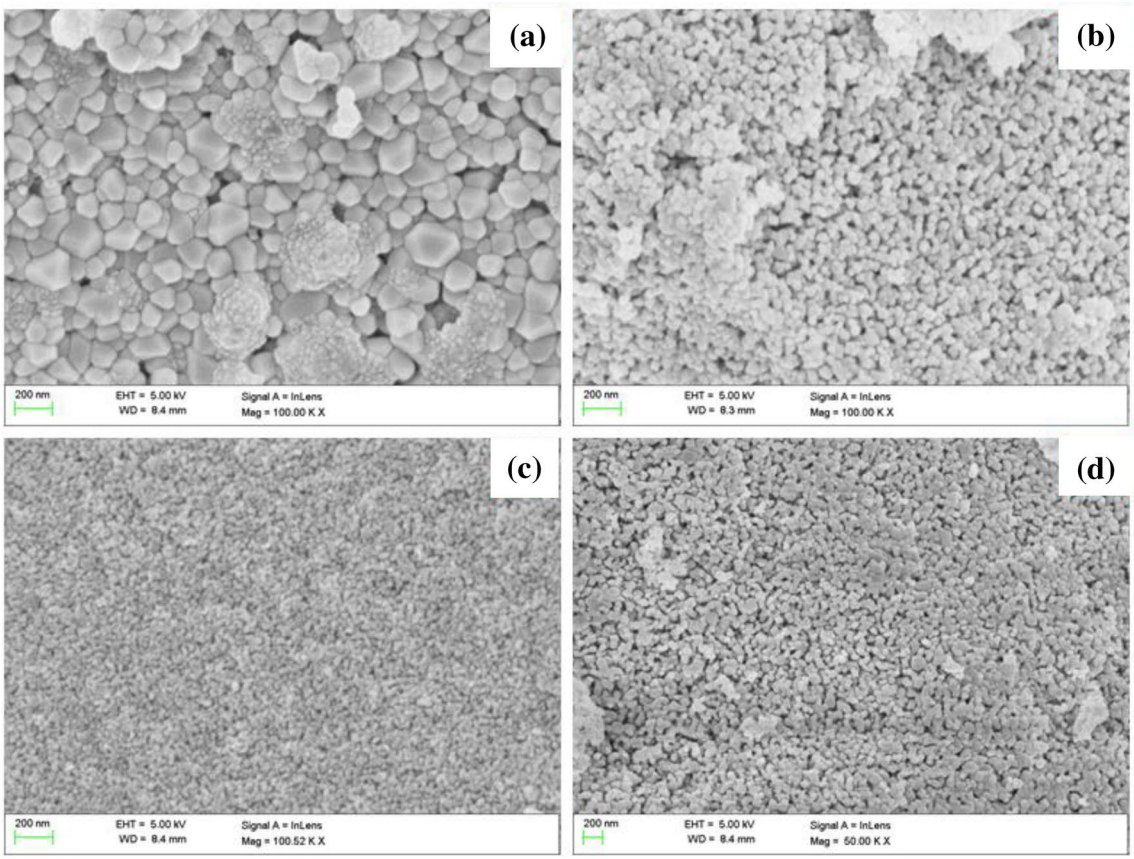

Fig. 4 **a**–**d** FESEM images of $Ni_{1-x}Ce_xO$ NPs for x = 0.0, 0.01, 0.02 and 0.03

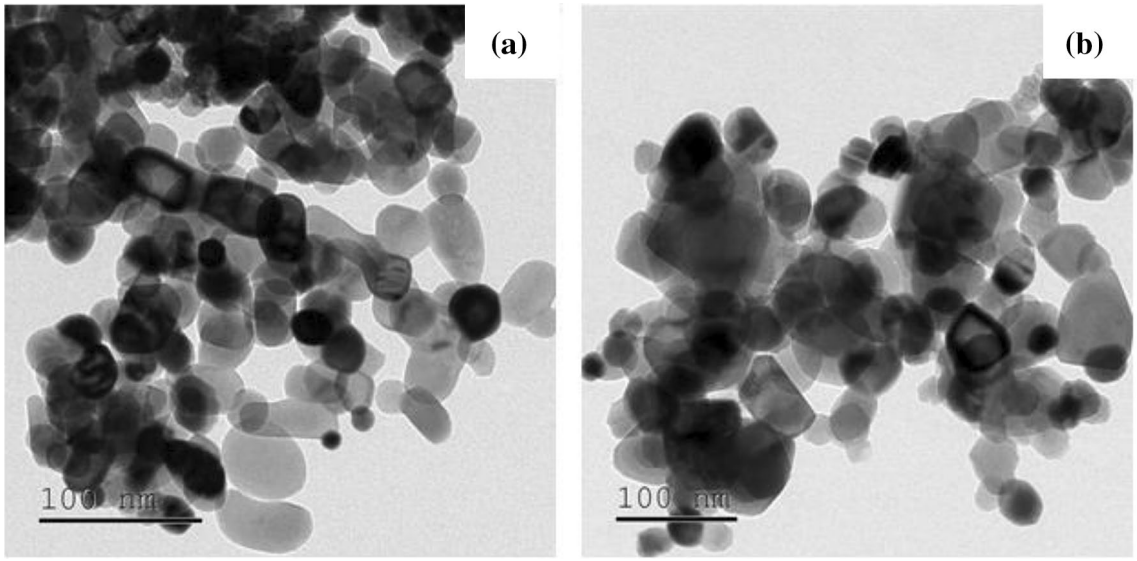

Fig. 5 **a**, **b** TEM images of NiO and $Ni_{0.097}Ce_{0.03}O$ NPs

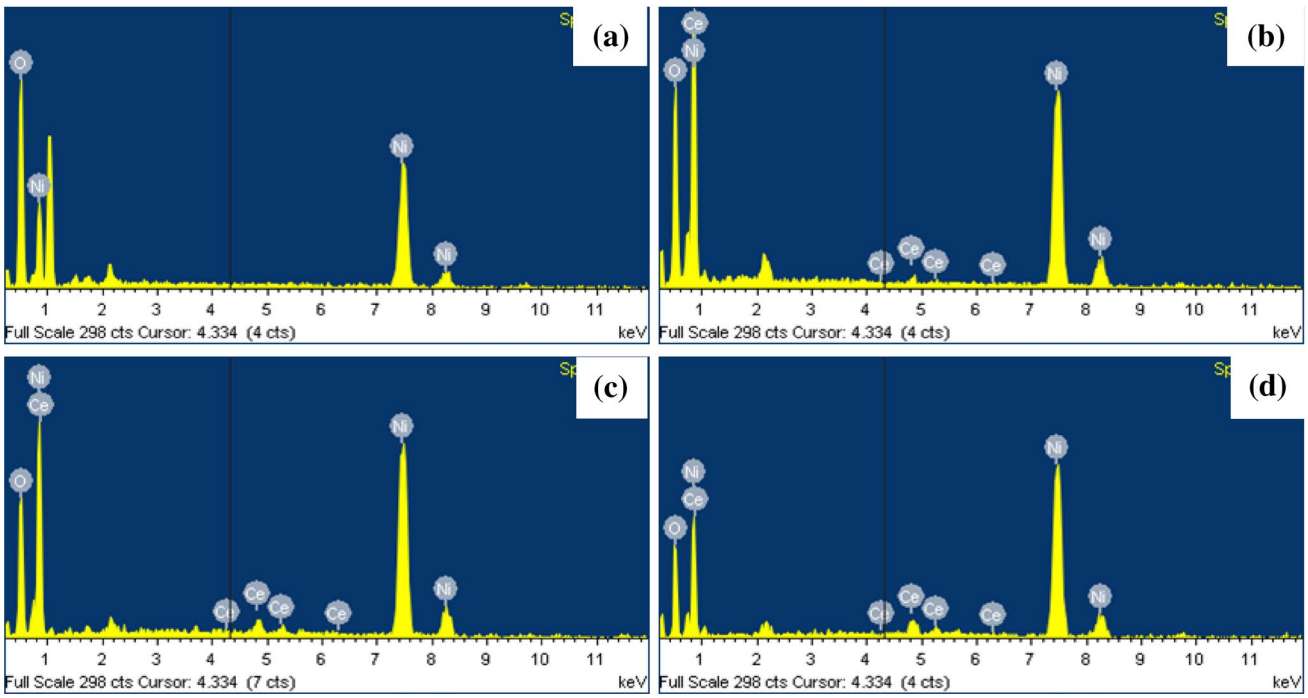

Fig. 6 **a**–**d** EDAX spectra of $Ni_{1-x}Ce_xO$ nanoparticles for x = 0.0, 0.01, 0.02 and 0.03

observed at 527 nm, this is due to the defects originated from the NiO lattice such as cation vacancies, interstitial oxygen trapping, and nickel vacancies produced by charge transfer between Ni^{2+} and Ni^{3+} ions [24, 25]. The intensities of peak decreased with the increase in Ce content. This doping effect produced a large variation inside the NiO nanoparticles active sites and it formed nickel interstitials (N_i), and oxygen vacancies (V_O). This may be due to the predominant of Ce^{3+} ionic effect [25].

Figure 11 shows the VSM analysis of A1 and A3 samples. The A1 sample exhibits super paramagnetic behavior and A3 exhibits ferromagnetic behavior at room temperature. The saturation magnetization values (Ms) were observed at 0.002 and 0.004 emu/g for NiO and Ce doped

Table 2 Elemental composition of NiO and Ce doped NiO NPs

Sample	Weight %			
	Ni	O	Ce	Total
A1	55.49	44.51	–	100
A2	53.48	45.69	0.60	100
A3	51.68	47.03	1.29	100
A4	50.07	48.34	1.67	100

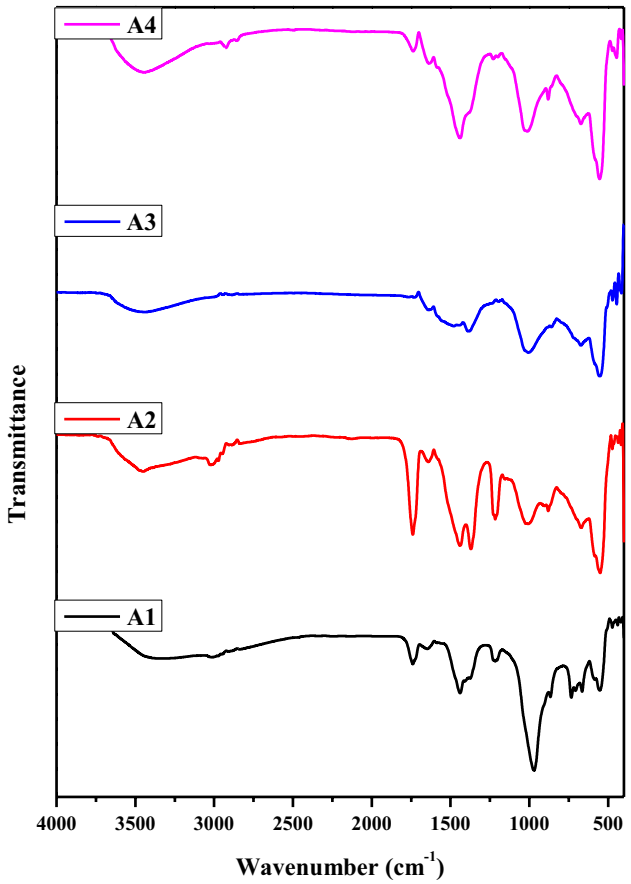

Fig. 7 FT-IR spectra of of $Ni_{1-x}Ce_xO$ nanoparticles for x = 0.0, 0.01, 0.02 and 0.03

NiO nanoparticles. The magnetization values of A3 are enhanced as compared to A1 sample due to the Ce^{3+} ions substitution in NiO matrix. This magnetic contribution may be the orientation of strong exchange interaction in s–f couple with Ce ions.

The antibacterial activities of A1, A2, A3 and A4 samples tested against(G+) bacteria *S. aureus* and *S. pneumoniae* and (G−) bacteria *E. coli*, *P. aeruginosa*, *P. vulgaris*, *K. pneumonia* and *S.dysenteriae are* studied by the well diffusion method as shown in Fig. 12. The A1, A2, A3, A4 and Erythromycin showed the antibacterial activity. The Zone inhibition of bacterial cells may be due to distractions of cell

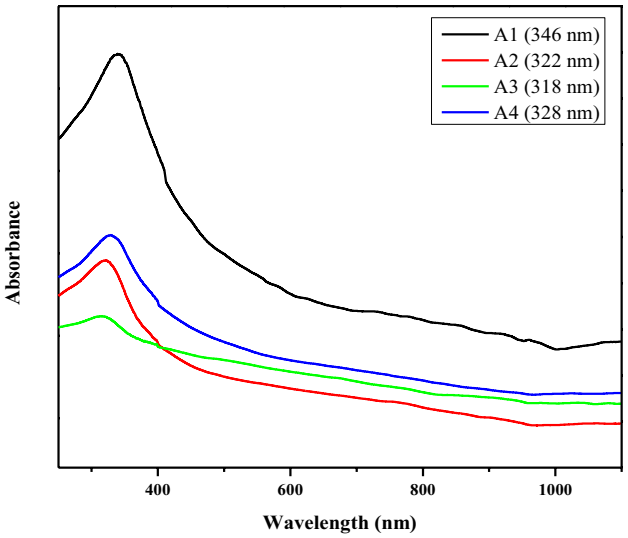

Fig. 8 UV–Vis absorption spectra of of $Ni_{1-x}Ce_xO$ nanoparticles for x = 0.0, 0.01, 0.02 and 0.03

membrane, is mainly due to the combination of various factors such as ROS and the release of Ni^{2+}, bacteria losing the viability of cell division, finally bacterial cells are death [26–29]. The schematic diagram of antibacterial mechanism is shown in Fig. 13. The *S. aureus*, *E. coli*, *K. pneumonia and S. dysenteriae bacteria* caused serious infections for human system such as breathing problem, dysentery, anemia or kidney failure, wound infections and urinary tract infections [30–33]. However, the synthesized A1, A2, A3 and A4 samples have been used for curing pneumonia, bloodstream infection, kidney failure, wound infection and urinary tract infections.

4 Conclusions

In summary, NiO and Ce doped NiO nanoparticles were prepared through chemical method. The XRD pattern revealed that the synthesized nanoparticles exhibited cubic structure. The oxidation states of Ni (2p) Ce (3d) and O (1s) were identified by x-ray photoelectron spectroscopy spectra for NiO NPs. The morphology were identified through FESEM and TEM analysis. The chemical compositions were identified through EDAX analysis. FT-IR spectra explained Ni–O stretching vibration observed at 439, 435, 445, and 446 cm^{-1} for respective NiO nanoparticles. The UV–Vis absorption spectra showed the absorption peak edges which are observed at 346, 322, 318 and 328 nm in A1, A2, A3 and A4 samples. The Ce doping of NiO NPs altered the band emission as compared to NiO NPs due to Nickel vacancies, oxygen vacancies and surface defects. The enhanced

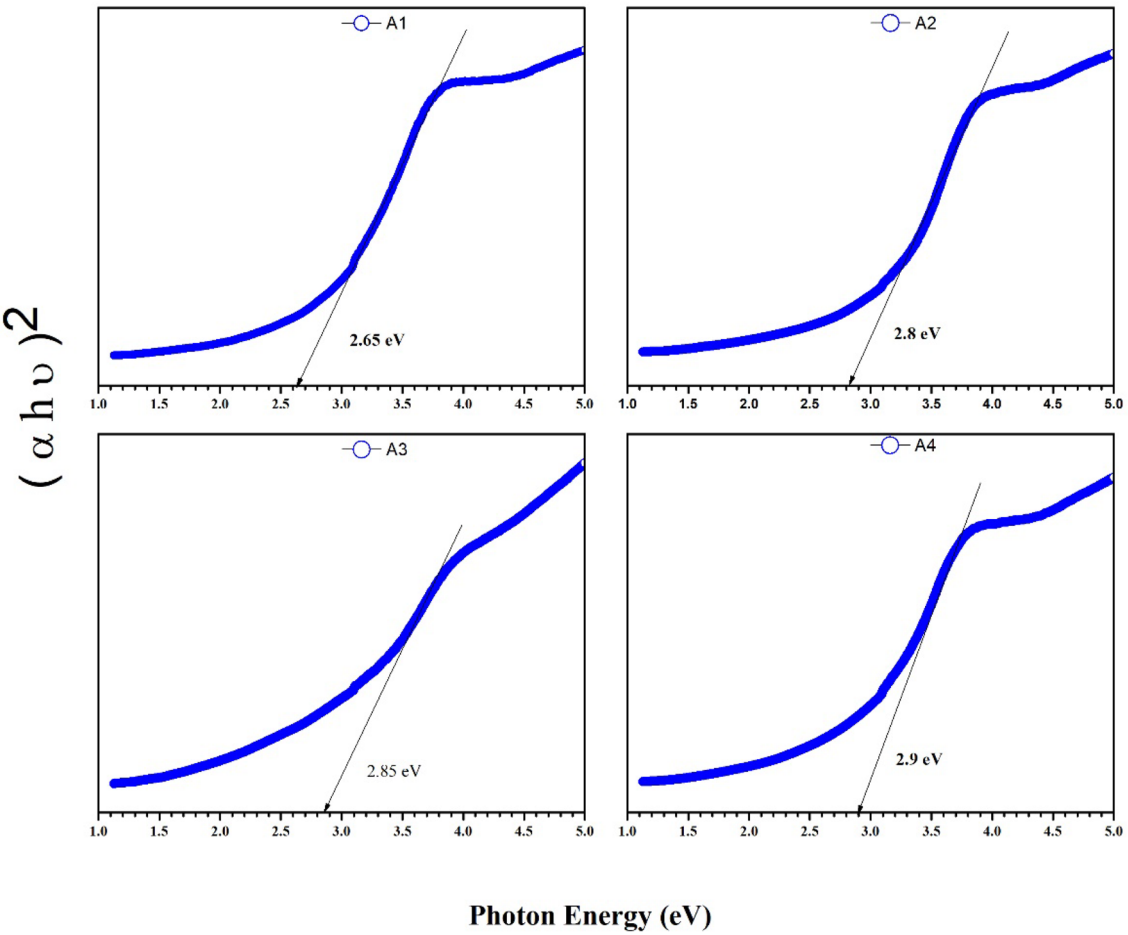

Fig. 9 Photon energy values of $Ni_{1-x}Ce_xO$ nanoparticles for x = 0.0, 0.01, 0.02 and 0.03

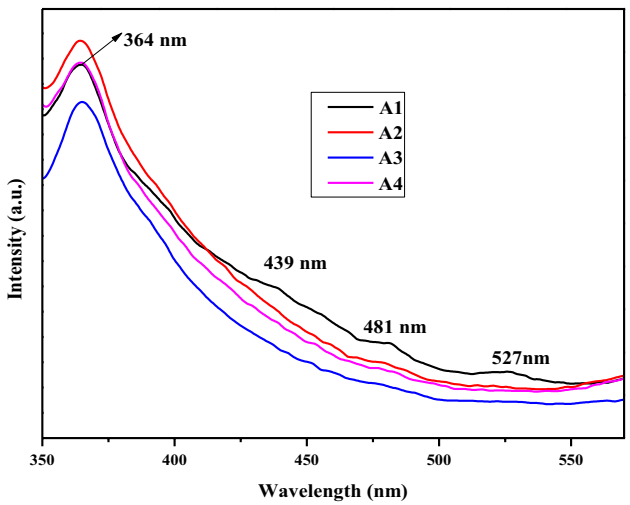

Fig. 10 PL spectra of $Ni_{1-x}Ce_xO$ nanoparticles for x = 0.0, 0.01, 0.02 and 0.03

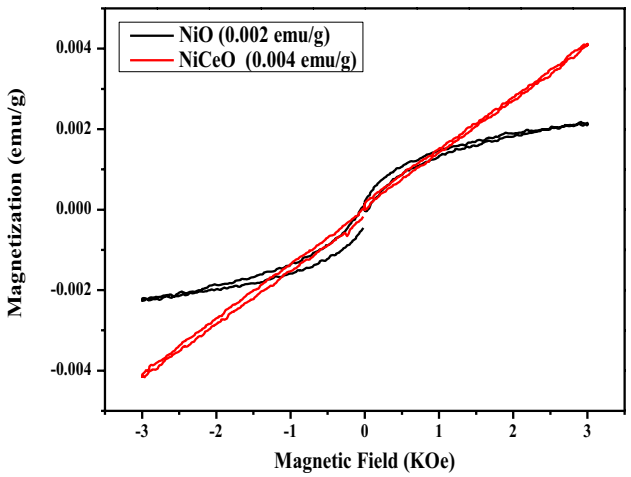

Fig. 11 Hysteresis curve of NiO and Ce doped NiO nanoparticles

magnetization values of Ce doped NiO NPs are more than that of NiO NPs, which was due to Ce^{3+} ions substitution in NiO matrix. The NiO, Ce doped NiO NPs and

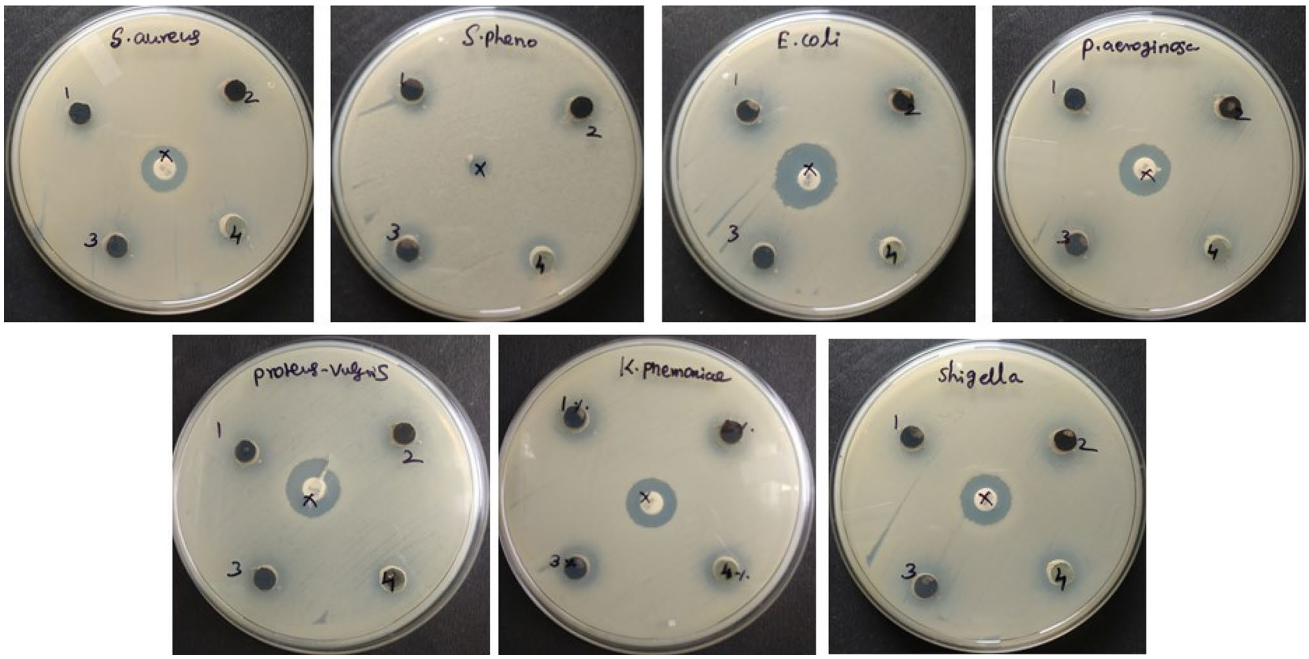

Fig. 12 The progressive antibacterial activity of $Ni_{1-x}Ce_xO$ nanoparticles for x = 0.0, 0.01, 0.02 and 0.03 against Gram-positive (*S. aureus* and *S. pneumoniae*) and Gram-negative bacteria (*E. coli*, *P. aeruginosa*, *P. vulgaris*, *K. pneumonia* and *S. dysenteriae*)

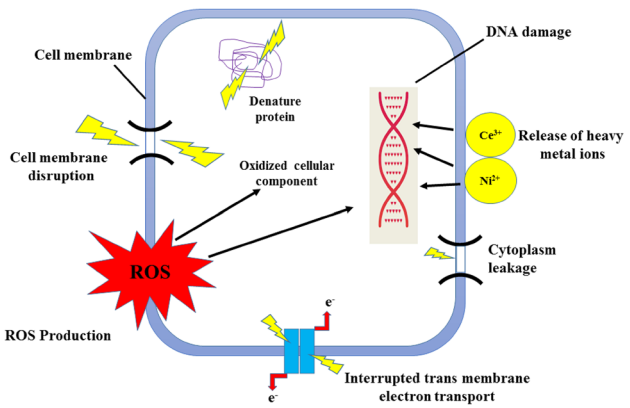

Fig. 13 Antibacterial activity of Ce doped NiO nanoparticles against bacterial pathogens

Erythromycin exhibited antibacterial activity. We suggest that synthesized NiO and Ce doped NiO nanoparticles can be used for the treatment of various human diseases such as pneumonia, bloodstream infection, kidney failure, wound infection and urinary tract infections.

Author contributions Mr. MAR carried out the preparation of nanoparticles and executes the physical characterization studies and contributed to the main text of the manuscript. Dr. RRK checked the scientific information and flow of the text to maintain a better readability. Further this research work is not funded by any agency.

Compliance with ethical standards

Conflict of interest The authors declared that they have no conflict of interest.

References

1. Rahman MA, Radhakrishnan R, Gopalakrishnan R (2018) Structural, optical, magnetic and antibacterial properties of Nd doped NiO nanoparticles prepared by co-precipitation method. J Alloys Compd 742:421–429
2. Du YP, Zhang YW, Sun LD, Yan CH (2008) Efficient energy transfer in monodisperse Eu-doped ZnO nanocrystals synthesized from metal acetylacetonates in high-boiling solvents. J Phys Chem C 112:12234–12241
3. Flor J, de Lima SAM, Davolos MR (2004) Effect of reaction time on the particle size of ZnO and ZnO: Ce obtained by a sol–gel method. Prog Colloid Polym Sci 128:239–243
4. Zeng XY, Yuan JL, Wang ZY, Zhang LD (2007) Nanosheet-based microspheres of Eu^{3+}-doped ZnO with efficient energy transfer from ZnO to Eu^{3+} at room temperature. Adv Mater 19:4510–4514
5. Wang X, Kong XG, Yu Y, Sun YJ, Zhang H (2007) Effect of annealing on upconversion luminescence of ZnO:Er^{3+} nanocrystals and high thermal sensitivity. J Phys Chem C 111:15119–15124
6. Walkey C, Das S, Seal S, Erlichman J, Heckman K, Ghibelli L, Traversa E, McGinnis JF, Self WT (2015) Catalytic properties and biomedical applications of cerium oxide nanoparticles. Environ Sci Nano 2(1):33–53
7. Ivanov VK, Shcherbakov AB, Usatenko AV (2009) Structure-sensitive properties and biomedical applications of nanodispersed cerium dioxide. Russ Chem Rev 78(9):855

8. Xu C, Qu X (2014) Cerium oxide nanoparticle: a remarkably versatile rare earth nanomaterial for biological applications. NPG Asia Mater 6(3):e90
9. Yang H, Tao Q, Zhang X, Tang A, Ouyang J (2008) Solid-state synthesis and electrochemical property of SnO 2/NiOnanomaterials. J Alloys Compd 459(1):98–102
10. Bahadur J, Sen D, Mazumder S, Ramanathan S (2008) Effect of heat treatment on pore structure in nano-crystalline NiO: a small angle neutron scattering study. J Solid State Chem 181(5):1227–1235
11. Hotovy I, Huran J, Spiess L, Hascik S, Rehacek V (1999) Preparation of nickel oxide thin films for gas sensors applications. Sensors Actuators B Chem 57(1):147–152
12. Nathan T, Aziz A, Noor AF, Prabaharan SR (2008) Nanostructured NiO for electrochemical capacitors: synthesis and electrochemical properties. J Solid State Electrochem 12(7–8):1003–1009
13. Granqvist CG (ed) (1995) Handbook of inorganic electrochromic materials. Elsevier, New York
14. Pankhurst QA, Connolly J, Jones SK, Dobson JJ (2003) Applications of magnetic nanoparticles in biomedicine. J Phys D Appl Phys 36(13):R167
15. Sun C, Lee JS, Zhang M (2008) Magnetic nanoparticles in MR imaging and drug delivery. Adv Drug Deliv Rev 60(11):1252–1265
16. Li QL, Mahendra S, Lyon DY, Brunet L, Liga MV, Li D, Alvarez PJJ (2008) Antimicrobial nanomaterials for water disinfection and microbial control: potential applications and implications. Water Res 42:4591–4602
17. Foster HA, Ditta IB, Varghese S, Steele A (2011) Photocatalytic disinfection using titanium dioxide: spectrum and mechanism of antimicrobial activity. Appl Microbiol Biotechnol 90:1847–1868
18. Wilson WW, Wade MM, Holman SC, Champlin FR (2001) Status of methods for assessing bacterial cell surface charge properties based on zeta potential measurements. J Microbiol Methods 43:153–164
19. Hattori Y, Konishi T, Kaneko K (2002) XAFS and XPS studies on the enhancement of methane adsorption by NiO dispersed ACF with the relevance to structural change of NiO. Chem Phys Lett 355(1):37–42
20. Salavati-Niasari M, Mir N, Davar F (2010) A novel precursor in preparation and characterization of nickel oxide nanoparticles via thermal decomposition approach. J Alloys Compd 493(1):163–168
21. Zandi S, Kameli P, Salamati H, Ahmadvand H, Hakimi M (2011) Microstructure and optical properties of ZnO nanoparticles prepared by a simple method. Physica B 406(17):3215–3218
22. Vallée C, Goullet A, Granier A, Van der Lee A, Durand J, Marliere C (2000) Inorganic to organic crossover in thin films deposited from O2/TEOS plasmas. J Non-Cryst Solids 272(2):163–173
23. Meybodi SM, Hosseini SA, Rezaee M, Sadrnezhaad SK, Mohammadyani D (2012) Synthesis of wide band gap nanocrystalline-NiO powder via a sonochemical method. Ultrasonicssonochemistry 19(4):841–845
24. Karthikeyan B, Pandiyarajan T, Hariharan S, Ollakkan MS (2016) Wet chemical synthesis of diameter tuned NiO microrods: microstructural, optical and optical power limiting applications. CrystEngComm 18:601–607
25. Hagfeldt A, Graetzel M (1995) Light-induced redox reactions in nanocrystalline systems. Chem Rev 95(1):49–68
26. Al-Tuwirqi R, Al-Ghamdi AA, Aal NA, Umar A, Mahmoud WE (2011) Facile synthesis and optical properties of Co_3O_4 nanostructures by the microwave route. Superlattices Microstruct 49:416–421
27. Kasinathan K, Kennedy J, Elayaperumal M, Henini M, Malik M (2016) Photodegradation of organic pollutants RhB dye using UV simulated sunlight on ceria based TiO2 nanomaterials for antibacterial applications. Sci Rep 6(1):38064
28. Javid A, Kumar M, Yoon S, Lee JH, Han JG (2017) Size-controlled growth and antibacterial mechanism for Cu: C nanocomposite thin films. Phys Chem Chem Phys 19:237–244
29. Tiwari V (2014) Anti-bacterial activity of polyvinyl pyrrolidone capped silver nanoparticles on the carbapenem resistant strain of *Acinetobacter baumannii*. J Nanomed Nanotechnol 5(06):1
30. Santhoshkumar A, Kavitha HP, Suresh R (2016) Hydrothermal synthesis, characterization and antibacterial activity of NiO nanoparticles. J Adv Chem Sci 24:230–232
31. Klebsiella pneumoniae in Healthcare Settings. Centers for Disease Control and Prevention. August 27, 12; http://www.cdc.gov/HAI/organisms/klebsiella/klebsiella.html. Accessed 5 June 2015
32. Besser RE, Lett SM, Weber JT, Doyle MP, Barrett TJ, Wells JG, Griffin PM (1993) An outbreak of diarrhea and hemolytic uremic syndrome from Escherichia coli O157: H7 in fresh-pressed apple cider. JAMA 269(17):2217–2220
33. Dealler SF, Hawkey PM, Millar MR (1988) Enzymatic degradation of urinary indoxyl sulfate by Providencia stuartii and Klebsiella pneumoniae causes the purple urine bag syndrome. J Clin Microbiol 26(10):2152–2156